LETTER

Fermi surfaces in Kondo insulators

To cite this article: Hsu Liu *et al* 2018 *J. Phys.: Condens. Matter* **30** 16LT01

View the article online for updates and enhancements.

Letter

Fermi surfaces in Kondo insulators

Hsu Liu[1,5], **Máté Hartstein**[1,5], **Gregory J Wallace**[1], **Alexander J Davies**[1], **Monica Ciomaga Hatnean**[2], **Michelle D Johannes**[3], **Natalya Shitsevalova**[4], **Geetha Balakrishnan**[2] and **Suchitra E Sebastian**[1]

[1] Cavendish Laboratory, Cambridge University, JJ Thomson Avenue, Cambridge CB3 0HE, United Kingdom
[2] Department of Physics, University of Warwick, Coventry CV4 7AL, United Kingdom
[3] Center for Computational Materials Science, Naval Research Laboratory, Washington, DC 20375, United States of America
[4] The National Academy of Sciences of Ukraine, Kiev 03680, Ukraine

E-mail: suchitra@phy.cam.ac.uk

CrossMark

Abstract

We report magnetic quantum oscillations measured using torque magnetisation in the Kondo insulator YbB_{12} and discuss the potential origin of the underlying Fermi surface. Observed quantum oscillations as well as complementary quantities such as a finite linear specific heat capacity in YbB_{12} exhibit similarities with the Kondo insulator SmB_6, yet also crucial differences. Small heavy Fermi sections are observed in YbB_{12} with similarities to the neighbouring heavy fermion semimetallic Fermi surface, in contrast to large light Fermi surface sections in SmB_6 which are more similar to the conduction electron Fermi surface. A rich spectrum of theoretical models is suggested to explain the origin across different Kondo insulating families of a bulk Fermi surface potentially from novel itinerant quasiparticles that couple to magnetic fields, yet do not couple to weak DC electric fields.

Keywords: Fermi surface, quantum oscillations, Kondo insulator

(Some figures may appear in colour only in the online journal)

Introduction

Evidence for a bulk Fermi surface in the Kondo insulator SmB_6 has been observed from a variety of experimental techniques, spanning quantum oscillations in the torque magnetisation [1–3], finite linear specific heat [1, 2, 4, 5], oscillatory magnetic entropy [2], and magnetic field enhanced thermal conductivity [2, 6]. A remarkable possibility is that the existence of a Fermi surface is more universal to correlated insulators. The observation of a Fermi surface in multiple families of correlated insulators would support a new paradigm that is distinct from the traditional idea where Fermi surfaces are the preserve of Fermi liquids. Here, we experimentally explore the possibility of a bulk Fermi surface in the Kondo insulator YbB_{12}, a material that is closely related to SmB_6 [7].

Kondo insulators are characterised by an energy gap arising from collective *f*-electron-conduction electron hybridisation, as schematically shown in figure 1(a) [8]. In the case of the Kondo insulator YbB_{12}, collective hybridisation occurs between the *f*-electron band and two conduction electron bands (shown in figure 4(a)), leading to a complex hierarchy of gaps. A small indirect gap of size ≈ 5 meV in YbB_{12}, similar in size to that in SmB_6, is determined from electrical transport measurements (figures 1(a) and (b), [9, 10]), accompanied by a larger direct hybridisation gap of ≈ 200 meV (figure 1(a)) accessed by complementary measurements such as optical spectroscopy [11] and tunneling spectroscopy [12]. Early observations of a finite linear term in the specific heat capacity (figure 1(d), [13]) and a finite density of states
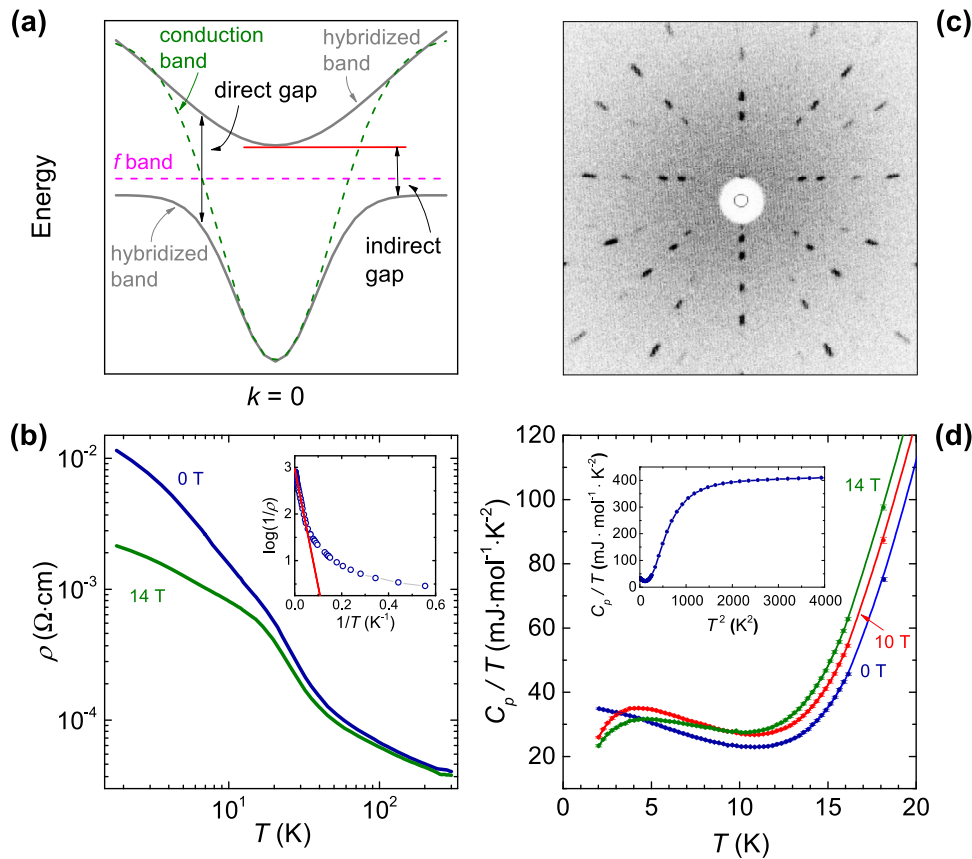
Figure 1. (a) Schematic depiction of the gap formation in a Kondo insulator by collective hybridisation of the *f*-electron and conduction electron bands. (b) Measured electrical resistivity as a function of temperature in magnetic fields of 0 T and 14 T. The inset shows the exponential fit $1/\rho \propto \exp\left(-2\Delta/k_\mathrm{B}T\right)$ to the electrical resistivity ρ in YbB_{12} at 0 T, where Δ is the activation gap. The indirect hybridisation bandgap is found to be ≈ 5 meV. (c) X-ray Laue back reflection photograph of a crystal of YbB_{12} (on which measured quantum oscillations are shown in figure 2) along the [0 0 1] direction, showing single crystallinity. (d) Measured specific heat capacity divided by temperature of YbB_{12} at 0 T, 10 T, and 14 T. A finite linear specific heat coefficient at low temperatures is seen, similar to that observed in SmB_6 [1, 2, 4, 5]. The measured linear specific heat coefficient is similar to that reported in [13]. While the finite value of γ above the upturn is enhanced by a magnetic field, as would be expected for a reduction in the activation gap, the low temperature upturn in specific heat capacity is suppressed by a magnetic field, suggesting its correspondence to a secondary low energy scale such as that associated with magnetic impurities or magnetic excitons, which is suppressed by a magnetic field. The inset shows the zero-field specific heat capacity divided by temperature versus T^2 up to 63 K.

in tunneling experiments [10] led to broad debate about the Kondo insulating mechanism in these materials. In view of the itinerant low energy excitations revealed in the Kondo insulator SmB_6 by quantum oscillation measurements [1–3], we revisit this question by searching for quantum oscillations in the magnetic torque measured on single crystals of YbB_{12}.

Methods

The growth of single phase YbB_{12} is challenging given its peritectic phase diagram and decomposition into YbB_{66} beyond a very narrow temperature range, necessitating careful control of temperature and composition during the growth process [14, 15]. Source YbB_{12} powder was prepared in polycrystalline form by borothermal reduction of a mixture of Yb_2O_3 (99.998 mass % purity) and amorphous B (99.9 mass % purity) at 1700 °C under vacuum [16]. The material was then isostatically pressed into a cylindrical rod and sintered at 1600 °C in argon gas flow for several hours. Single crystal growth of YbB_{12} was carried out at the University of Warwick by the traveling solvent floating zone technique under

conditions similar to those previously reported in [14] using a four-mirror xenon arc lamp (3 kW) optical image furnace (Crystal Systems Incorporated, Japan). The growths were performed in a reducing atmosphere (Ar + 3% H_2) at a growth rate of 18 mm hr^{-1} with the feed and seed rods counter-rotating at 20–30 rpm. LuB_{12} single crystals were prepared at the National Academy of Sciences of Ukraine, Kiev by the inductive floating zone method as described in [16]. Laue x-ray imaging with a Multiwire Laue camera system was used to determine the quality of the grown crystal boules and to select and orient single crystal samples cut from the as-grown boule. Single crystals were selected that yielded high inverse electrical residual resistivity ratios (figure 1(b)) and well-defined spots in the Laue diffraction pattern, evidencing high single crystal quality (figure 1(c)). Elemental composition analysis was performed on selected single crystals using an FEI Philips XL30 sFEG scanning electron microscope (SEM) to reveal an atomic ratio between Yb and B closely comparable to the stoichiometric ratio of 1 : 12 and distinct from the ratios for YbB_6 and for YbB_{66}. Energy dispersive x-ray microanalysis on multiple samples provided comparable results to SEM.

Rietveld refinement performed using the Bruker TOPAS software on powder x-ray diffraction data yielded a lattice constant of 7.4686(1) Å, agreeing well with published data for YbB$_{12}$ [16].

Torque magnetisation measurements were made on YbB$_{12}$ and LuB$_{12}$ in DC magnetic fields at the University of Cambridge (up to 14 T) and at the National High Magnetic Field Laboratory (NHMFL) in Tallahassee (up to 45 T) using flexible T-shaped BeCu cantilevers of 20 or 50 μm thickness, with the narrow end anchored and the wide end floating above a fixed Cu film. Single crystals of dimensions approximately $1 \times 1 \times 0.5$ mm^3 were mounted on the wide end of the cantilever. The cantilever and the Cu film form the two plates of a capacitor whose capacitance is measured using a General Radio analogue capacitance bridge in conjunction with a Stanford Research Systems lock-in amplifier. The measured change in capacitance ΔC is proportional to the change in magnetic torque. Specific heat measurements were made using the standard heat capacity option for the Physical Property Measurement System from Quantum Design Inc (figure 1(d)).

Density functional theory Fermi surfaces were calculated with the WIEN2k augmented plane wave plus local orbital (APW + lo) code [17]. The modified Becke–Johnson (mBJ) potential was used, which is a semi-local approximation to the exact exchange plus a screening term [18] and which improves the band gap in many semiconductor materials. Application of mBJ resulted in a non-magnetic ground state with an indirect band gap of 21 meV and a direct gap of 80 meV, whereas the standard Perdew–Burke–Ernzerhof potential produced a semimetal with overlapping valence and conduction bands. Spin-orbit coupling was included via the second variational method and resulted in a strong reordering of the bands. Self-consistent calculations were converged using a k-mesh of $15 \times 15 \times 15$ followed by a non-self-consistent calculation with a $30 \times 30 \times 30$ mesh for calculation of Fermi surfaces. Extremal cross-sectional areas of the Fermi surfaces were calculated for the magnetic field in the [0 0 1], [1 1 0] and [1 1 1] cubic crystal directions using the open source visualization software, OpenDX. Effective masses were obtained by shifting the Fermi energy up/down by 0.7 meV from its original value, obtaining the new cross-sections and then calculating the cyclotron effective mass using the resulting finite differences.

Quantum oscillations in YbB$_{12}$

Figure 2(a) shows the magnetic torque measured on a single crystal of YbB$_{12}$ as a function of DC magnetic fields up to 45 T, from which a monotonic smooth background has been subtracted. Quantum oscillations periodic in inverse magnetic field are observed for magnetic field tilt angles θ spanning [0 0 1], [1 1 1] to [1 1 0] crystal directions, and extending down to magnetic fields at least as low as 22 T. An example Fourier transform of quantum oscillations in inverse magnetic field shown in figure 2(c) reveals multiple quantum oscillation frequencies between 300–1500 T. The quantum oscillation frequency >1 kT is seen most clearly in the high magnetic field

range (figure 2(c) inset). While this higher quantum oscillation frequency is close to a harmonic of lower frequency quantum oscillations, there is no obvious observation of frequencies corresponding to harmonics of dominant amplitude low frequency quantum oscillations. The temperature dependence of the measured quantum oscillation amplitude follows a Lifshitz–Kosevich (LK) form, yielding cyclotron effective masses of m^*/m_e between 3–10 for the various measured quantum oscillation frequencies (figure 2(d), [19, 20]). Figure 2(b) shows the angular dependence of the measured quantum oscillation frequencies for magnetic field tilt angles spanning [0 0 1], [1 1 1] to [1 1 0] crystal directions, which reveals only a subtle variation in quantum oscillation frequency as a function of angle, consistent with a three-dimensional Fermi surface geometry.

We calibrate the absolute amplitude of quantum oscillations we observe in YbB$_{12}$ in units of μ_B per Yb unit cell by using the spring constant of the cantilever used to make torque magnetisation measurements. The method to convert the measured capacitance to absolute units of magnetic torque is the same as that detailed in [2]. Keeping the notation consistent with [2], we have cantilever length $L = 3.1$ mm, distance between cantilever and fixed Cu plate $d_0 = 0.1$ mm, spring constant $k = 190$ N m^{-1}, lattice constant $a_{u.c.} = 0.747$ nm, and crystal volume $s^3 = 0.9 \times 0.5 \times 0.3$ mm^3. We thus convert the measured torque magnetisation in terms of capacitance (C) to an absolute magnetic moment p_s in units of Bohr magneton per unit cell by the expression:

$$\Delta p_s = \frac{20}{\mu_0 H \sin \theta_M} \cdot \Delta C \quad \text{T} \cdot \text{pF}^{-1} \; \mu_B \text{ per unit cell.} \quad (1)$$

Here, 20 T pF^{-1} is calculated with the parameters above according to [2], and θ_M is the angle between the magnetic field $\mu_0 H$ and the total magnetic moment.

We compare the measured size of the quantum oscillations to the theoretical LK estimate for a quantum oscillatory magnetic moment of bulk origin, including the angular anisotropy term, Dingle and spin-splitting damping factors as detailed in [2]. For the quantum oscillations observed in YbB$_{12}$, we use the experimentally measured values inferred from figure 2, and a Dingle damping factor $R_D = \exp(-100 \text{ T}/\mu_0 H)$. We find the expected theoretical amplitude of the magnetic moment for the $F \approx 300$ T frequency of YbB$_{12}$ to be of the order of $1 - 4 \times 10^{-4}$ μ_B per unit cell at $\mu_0 H = 45$ T. This theoretical estimate is comparable in order of magnitude to the experimentally measured amplitude of quantum oscillations shown in figure 3(a).

We consider a breadth of experimental observations to discern whether the observed quantum oscillations correspond to the bulk volume of the sample. Firstly, we find that the experimentally measured quantum oscillation amplitude (shown in figure 3) is in agreement with the theoretical estimate from the LK theory for quantum oscillations arising from the bulk volume of the sample, as calculated above. Secondly, we compare two samples with differing impurity concentrations, and examine whether the amplitude of quantum oscillations scales with the Dingle impurity term as would be expected for quantum oscillations arising from the
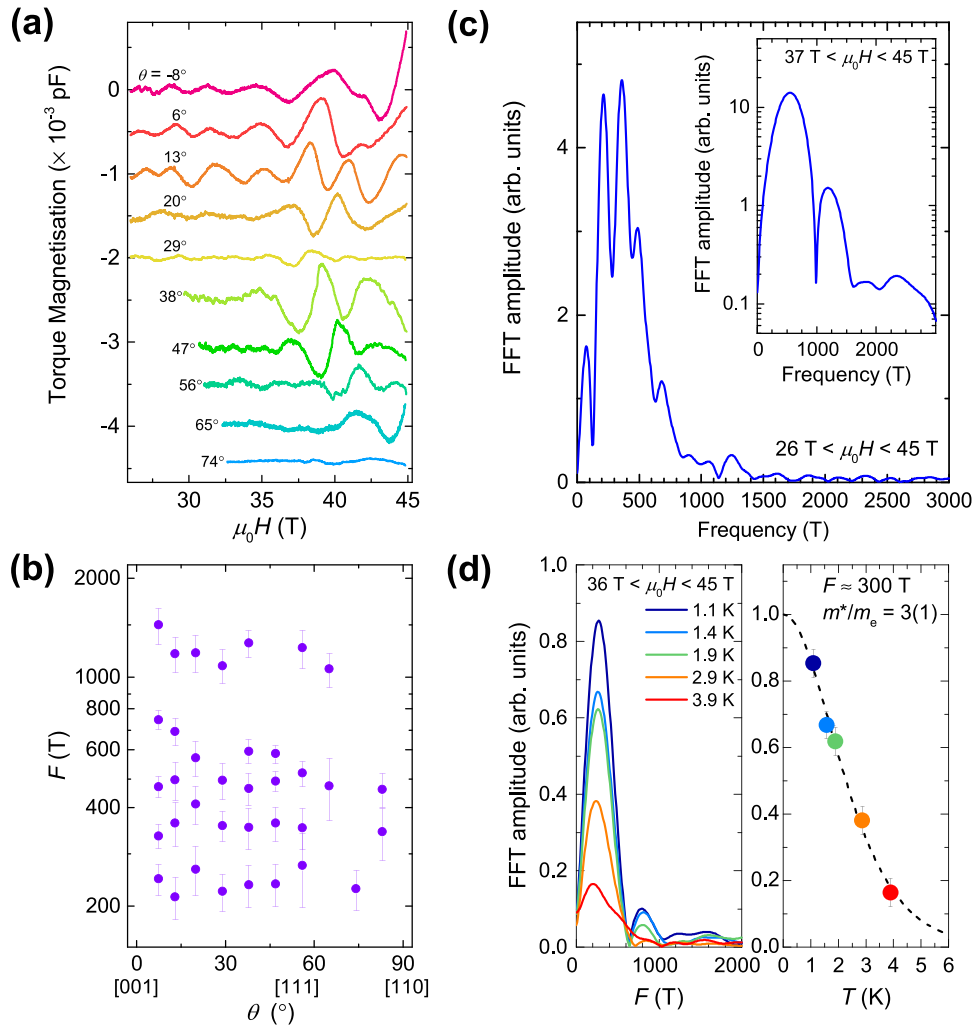
Figure 2. (a) Solid lines show de Haas–van Alphen oscillations measured on a single crystal of YbB$_{12}$ using torque magnetisation at $T = 0.4$ K for $\mu_0 H$ oriented at different tilt angles (θ) away from the [0 0 1] crystalline direction, passing through the [1 1 1] crystalline direction, and approaching the [1 1 0] crystalline direction. (b) Angular dependence of measured quantum oscillation frequencies for values of magnetic field tilt angle spanning the [0 0 1] crystalline direction, through the [1 1 1] crystalline direction, and approaching the [1 1 0] crystalline direction. (c) Example Fourier transform of the magnetic field sweep at $\theta \approx 13°$ showing quantum oscillation peaks for a magnetic field window between 26 T and 45 T. The inset shows the Fourier transform of the magnetic field sweep at $\theta \approx 13°$ for a high magnetic field window between 37 T and 45 T, more clearly showing the quantum oscillation peak at 1.2 kT. (d) Left panel shows an example Fourier transform at $\theta \approx 6°$ measured at different temperatures. Right panel shows the quantum oscillation amplitude obtained from the peak height of the Fourier transforms shown in the left panel, plotted as a function of temperature T. Performing an LK fit (shown by a dashed line) yields an effective mass of $m^*/m_e = 3(1)$.

bulk volume of the sample. We measure quantum oscillations in a single crystal of YbB$_{12}$ with more domains in the Laue pattern signaling grain boundaries or inclusions, and a lower value of inverse electrical residual resistivity ratio than the sample on which quantum oscillations are shown in figures 2 and 3. Quantum oscillations are observed on this sample, with a substantially higher Dingle impurity damping factor of $R_D = \exp(-300 \text{ T}/\mu_0 H)$. We find the amplitude of quantum oscillations observed in this single crystal with increased impurity levels to be more than an order of magnitude lower than the higher quality single crystal shown in figures 2 and 3, as expected for quantum oscillations originating from the bulk of the single crystal rather than from small secondary phase inclusions. Thirdly, we study the neighbouring semi-metal YbB$_6$ in the peritectic phase diagram, to examine the likelihood of the observed quantum oscillations arising from inclusions of this phase. We find that torque magnetisation

measurements on pure single crystals of YbB$_6$ yielded no discernible quantum oscillations up to an applied magnetic field of 14 T under similar experimental conditions of low temperature and high measurement sensitivity, making this an unlikely source of the quantum oscillations observed in single crystals of YbB$_{12}$. Fourthly, we note the quantum oscillation amplitude at the highest magnetic fields potentially shows a growth in amplitude beyond that expected solely from Dingle impurity damping for magnetic field tilt angles close to the [0 0 1] crystalline direction (figures 2(a) and 3(a)). Especially given that the magnetic field at which an insulator-metal transition occurs in YbB$_{12}$ is lowest (≈ 50 T) along the [0 0 1] crystalline direction [21], a rapid increase in quantum oscillation amplitude at high magnetic fields would be a natural consequence of the approach to an insulator-metal phase transition in bulk YbB$_{12}$, unlike in the case of a secondary phase inclusion.
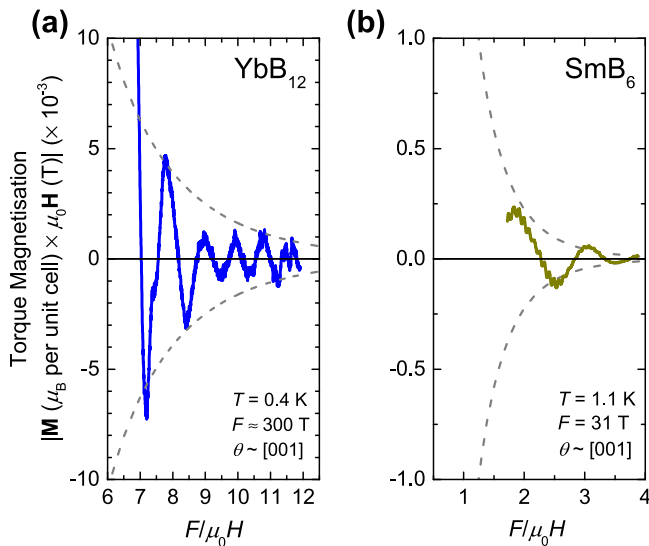
Figure 3. Quantum oscillatory magnetic moment (in μ_B per unit cell) corresponding to the measured oscillations versus inverse magnetic field in YbB_{12} in (a), and SmB_6 in (b) (reprinted by permission from Macmillan Publishers Ltd: Nature Physics [2], Copyright 2017). Dashed lines represent the calculated magnetic field dependence of the quantum oscillation amplitude from exponential Dingle damping, for a damping factor of ≈ 100 T in the case of YbB_{12}, and 30 T in the case of SmB_6. The theoretical LK estimate for the quantum oscillatory magnetic moment taking into account the angular anisotropy term, Dingle and spin-splitting damping factors is found to be $1–4 \times 10^{-4}$ μ_B per unit cell at $F/\mu_0 H = 6.9$ in the case of YbB_{12}, and $0.2–1 \times 10^{-4}$ μ_B per unit cell at $F/\mu_0 H = 1.9$ in the case of SmB_6.

Fermi surface origin in YbB_{12}

We explore band structure calculations to shed light on the origin of the Fermi surface observed in YbB_{12} yielding quantum oscillations with low frequency and high effective mass, in contrast to the quantum oscillations of both low and high frequency and low effective mass observed in SmB_6. Band structure calculations of YbB_{12} using the mBJ potential are shown in figure 4. States at both the valence band maximum and conduction band minimum are mainly derived from Yb f-states, but are heavily hybridised with the dispersive boron s and p states in the vicinity. We decompose the eigenvectors at each k-point both orbitally and atomically. Integrating over all k-points, we find, for the 14 states of the Yb f-complex, 13.2 below the Fermi energy and 0.8 above (figures 4(a) and (b)). Counting the empty states indicates 0.8 holes in the f-complex, consistent with a nominally Yb^{3+} semiconducting state that corresponds well with experiment [7] and band structure calculations that use a GW potential [22]. Interestingly, application of DFT + U, the most commonly used technique for dealing with metallic f-states, instead results in all 14 states being filled and corresponds to Yb^{2+}, which is inconsistent with experiment, as also found by previous band structure calculations [23]. A crucial distinction is therefore seen between the band structure of SmB_6 and YbB_{12}. In the case of SmB_6, the boron bands are filled and consequently a single half-filled unhybridised conduction d-electron band crosses the Fermi energy. Hybridisation of this conduction band with

the f-electron band yields the Kondo gap. In contrast, in the case of YbB_{12}, two partially filled unhybridised s-p conduction electron bands that are cumulatively half-filled cross the Fermi energy with electron-like character, and are gapped by hybridisation with the f-electron band as shown in figures 4(a) and (b).

Given the absence of a finite electronic density of states at the Fermi energy, constituent neutral quasiparticles have been proposed to explain the observation of a bulk Fermi surface in Kondo insulators. Neutral quasiparticles invoked by various theoretical models include spinons in the case of single band Mott insulating organic spin liquids [24–27], and in the case of single band Kondo insulators such as SmB_6, magnetic excitons [28], composite excitons [29, 30], Majorana fermions [31–33], and others [34, 35]. A natural way to think of a Fermi surface of such neutral quasiparticles is in terms of slow fluctuations in space and time between the insulating ground state where a Fermi surface is absent due to filling of the Brillouin zone, and the neighbouring metallised ground state in phase space, which is characterised by a Fermi surface [1, 2]. The character of such a neutral Fermi surface may thus be expected to be akin to the Fermi surface of the neighbouring metallised ground state. Metallisation in the case of SmB_6 requires a decoupling of the f-electron and conduction electron bands, resulting in a solely conduction electron Fermi surface occupying half the Brillouin zone. Accordingly, comparison of the observed Fermi surface in insulating SmB_6 with a conduction electron Fermi surface similar to that in metallic LaB_6 was found to yield good agreement both in frequency and effective mass [1, 2]. In contrast, metallisation of YbB_{12} can arise through two routes: either (i) a decoupling of the f-electron and conduction electron bands yielding a Fermi surface corresponding to the conduction electron band, or (ii) an effective relative shift of each of the two hybridised conduction electron bands, yielding a Fermi surface corresponding to a heavy fermion semimetal [29, 30].

We consider the first scenario, and make a comparison of the small heavy Fermi surface sections observed in insulating YbB_{12} with a conduction electron Fermi surface similar to that in metallic LuB_{12}. In LuB_{12}, all 14 f-states are well below the Fermi energy in the calculated band structure, resulting in a metallic ground state with highly dispersive boron bands and light carriers (figure 5(a), [36, 37]). Quantum oscillations we measured using torque magnetisation in LuB_{12} (shown in figures 5(e)–(g)) yield good agreement with the calculated band structure (figures 5(a)–(d)), and with previous quantum oscillation measurements [36, 38]. A correspondence is not immediately obvious between the observed quantum oscillations with a relatively high effective mass in YbB_{12} (figure 2(d)) and the large and light conduction electron Fermi surface expected from band structure and observed in LuB_{12} (figure 5). It is possible that owing to subtle materials differences between YbB_{12} and LuB_{12}, a band shift could yield small Fermi surface pockets from the conduction electron band similar to those observed in YbB_{12}. Meanwhile, quantum oscillations corresponding to large Fermi surface pockets might not be observed due to even higher effective masses than for the small Fermi surfaces observed. Alternatively, in the second scenario, metallisation in YbB_{12} can be achieved by a small effective relative shift of the two conduction bands while retaining hybridisation or potentially reduced hybridisation. In
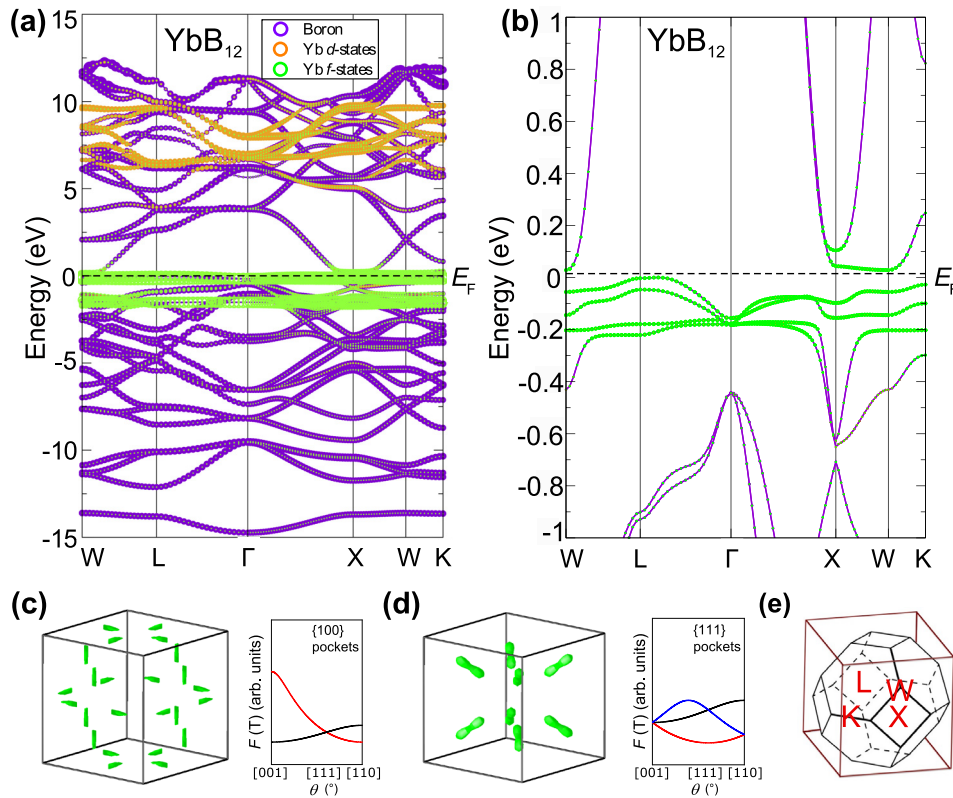
Figure 4. Calculated band structure of YbB$_{12}$ shown over a wide energy range in (a) with an expanded view around the Fermi energy E_F in (b). Several characters are projected out of the eigenvectors at each k-point and the resulting weight is indicated by a circle of proportional size. Green circles are Yb f-states, orange circles are Yb d-states, and violet circles are boron states. (c) Small needle-shaped Fermi surfaces of YbB$_{12}$ with effective mass $m^*/m_e \approx 6$ obtained using the modified Becke–Johnson potential for a small positive energy shift. Expected angular dependence of the quantum oscillation frequencies in the [0 0 1]-[1 1 1]-[1 1 0] rotation plane are shown by approximating the shown Fermi surfaces as prolate ellipsoids. (d) Small peanut-shaped Fermi surfaces of YbB$_{12}$ with effective mass $m^*/m_e \approx 9$ obtained using the modified Becke–Johnson potential for a small negative energy shift. Expected angular dependence of the quantum oscillation frequencies in the [0 0 1]-[1 1 1]-[1 1 0] rotation plane are shown by approximating the shown Fermi surfaces as prolate ellipsoids. (e) A schematic of the conventional face-centred cubic Brillouin zone used for the band structures within the cubic Brillouin zone used for the Fermi surfaces.

this case, small heavy Fermi surface sections characteristic of a heavy fermion semimetal [8] would be expected, as can be seen from performing small energy shifts to the band structure (figures 4(c) and (d)). Such heavy Fermi surface sections would also yield a sizable linear heat capacity as observed in YbB$_{12}$ (figure 1(d), [13]). This scenario of a neutral Fermi surface in Kondo insulating YbB$_{12}$ with properties similar to the Fermi surface of a heavy fermion semimetal, arising from a small relative shift to the two hybridised conduction bands, is intriguing to pursue theoretically. The realm of Fermi surfaces in Kondo insulators may be even richer than previously thought. Just as materials differences between metals yield differences in band structure and consequently Fermi surface character, we find that differences between the nature of f-electron and conduction electron hybridisation in SmB$_6$ and YbB$_{12}$ yield potentially important differences in Fermi surface character between the two Kondo insulators.

Magnetic field tuning in YbB$_{12}$

Another salient difference between SmB$_6$ and YbB$_{12}$ is the effectiveness of magnetic field in tuning these materials toward an insulator–metal transition. While applied magnetic

fields as high as $\mu_0 H = 93$ T only result in a negative magnetoresistance of $\approx 7\%$ in SmB$_6$ [39], applied magnetic fields of $\mu_0 H \approx 45$ T are found to reduce the electrical resistivity by an order of magnitude in YbB$_{12}$ (figure 1(b), [21]). The enhanced response of YbB$_{12}$ to applied magnetic fields compared to SmB$_6$ may reflect small band shifts due to Zeeman splitting or the involvement of magnetic degrees of freedom in the ground state of YbB$_{12}$. The close proximity of YbB$_{12}$ to the insulator-metal transition may be expected to lead to an increased propensity for quantum oscillations originating from neutral quasiparticles [24–27, 29–33]. Such an effect would yield larger amplitude quantum oscillations at higher magnetic fields, potentially yielding the increase in quantum oscillation amplitude beyond that expected from Dingle damping suggested from the experimental data for magnetic field tilt angles near the [0 0 1] crystalline direction in YbB$_{12}$ (figures 2(a) and 3(a)). Alternatively, the reduced charge gap at high magnetic fields could also provide an explanation in terms of conventional quasiparticles tunneling through a narrow energy gap that are more likely to yield quantum oscillations [40–43]. Taken in conjunction with the observation of a finite linear specific heat capacity (figure 1(d), [13]) even in zero magnetic field, an explanation for the observed quantum oscillations in terms of a Fermi surface originating from novel
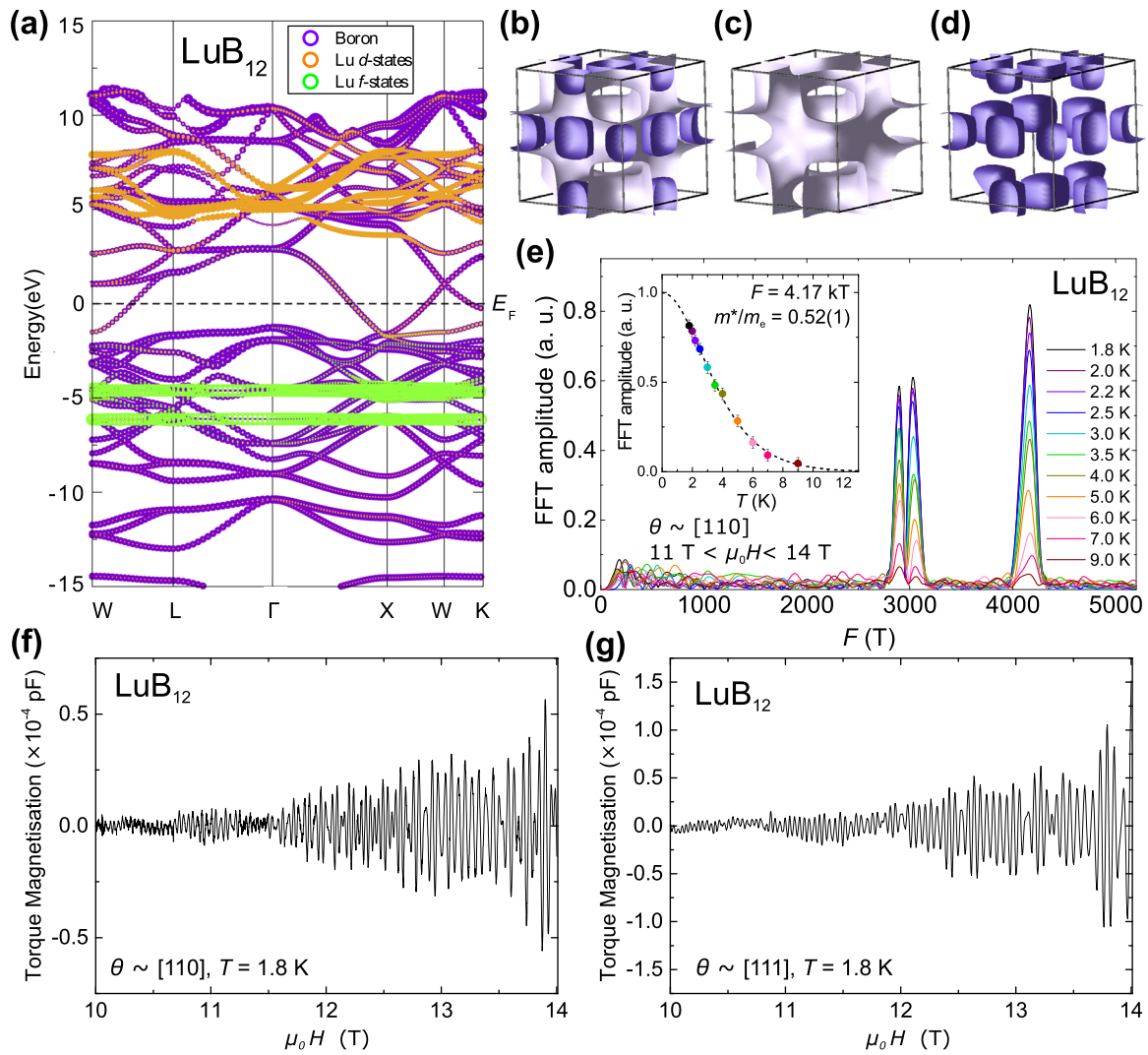
Figure 5. (a) Calculated band structure of LuB_{12}. Several characters are projected out of the eigenvectors at each k-point and the resulting weight is indicated by a circle of proportional size. Green circles are Lu f-states, orange circles are Lu d-states, and violet circles are boron states. (b)–(d) The Fermi surfaces of LuB_{12} shown together in (b) and separately for clearer viewing in (c) and (d). (f)–(g) De Haas–van Alphen oscillations measured using torque magnetisation at 1.8 K in LuB_{12}. (e) Fourier transform of the magnetic field sweeps taken at different temperatures. The inset shows the LK fit (dashed line) to the frequency $F = 4.17$ kT. The effective masses m^*/m_e are found to be 0.40(1), 0.53(2), and 0.52(1) for the frequencies 2.90 kT, 3.03 kT, and 4.17 kT for $\mu_0 H$ oriented a few degrees away from [1 1 0], corresponding well to calculated frequencies 2.92 kT and 3.93 kT for $\mu_0 H \parallel$ [1 1 0] with effective masses m^*/m_e of 0.36 and 0.43 respectively. Frequencies 2.89 kT, 3.51 kT, 3.75 kT, and 5.64 kT are measured for $\mu_0 H$ oriented a few degrees away from [1 1 1], comparable to calculated frequencies of 2.82 kT and 5.80 kT for $\mu_0 H \parallel$ [1 1 1] with effective masses m^*/m_e of 0.35 and 0.67 respectively.

quasiparticles that couple to a magnetic field but not to a weak DC electric field appears more likely than an origin from conventional tunneling through a magnetic-field reduced charge gap.

Summary

The observation of magnetic quantum oscillations in at least two families of Kondo insulators, SmB_6 and YbB_{12}, suggests a more universal phenomenon across correlated insulators. Differences we uncover between the character of the underlying bulk Fermi surface in the two systems further add to the richness of potential Fermi surface models relevant to the broad panorama of Kondo insulators. While the Fermi surface observed in SmB_6 corresponds in geometry and effective mass

to the conduction electron Fermi surface, the Fermi surface observed in YbB_{12} corresponds more closely to that of a heavy fermion semimetal, suggesting important differences between theoretical models of relevance to each of these systems. The magnetic field tuning we find to influence the quantum oscillations observed in YbB_{12}, while having little effect on the quantum oscillations in SmB_6, further informs our understanding of the itinerant low energy excitations involved in each of these materials and their approach to the neighbouring insulator–metal quantum critical point. Looking ahead, magnetic field dependent quantum oscillation measurements in other quantities, as well as complementary measurements such as thermal conductivity and nuclear magnetic resonance at low temperatures, are important in the quest to examine the character of the novel itinerant low energy excitations in YbB_{12}. Our results provide further impetus to the search

underway for new theoretical paradigms to explain the unexpected discovery of a bulk Fermi surface in Kondo insulating materials [24–27, 29–33, 40–43].

ORCID iDs

Máté Hartstein ⦿ https://orcid.org/0000-0003-1128-8057
Monica Ciomaga Hatnean ⦿ https://orcid.org/0000-0003-2870-8847
Suchitra E Sebastian ⦿ https://orcid.org/0000-0002-1386-8138

References

[1] Tan B S *et al* 2015 *Science* **349** 287–90
[2] Hartstein M *et al* 2018 *Nat. Phys.* **14** 166–72
[3] Li G *et al* 2014 *Science* **346** 1208–12
[4] Flachbart K, Gabáni S, Neumaier K, Paderno Y, Pavlík V, Schuberth E and Shitsevalova N 2006 *Physica* B **378–80** 610–1
[5] Gabáni S, Flachbart K, Konovalova E, Orendáč M, Paderno Y, Pavlík V and Šebek J 2001 *Solid State Commun.* **117** 641–4
[6] Boulanger M E *et al* 2017 arXiv:1709.10456
[7] Kasaya M, Iga F, Takigawa M and Kasuya T 1985 *J. Magn. Magn. Mater.* **47–8** 429–35
[8] Hewson A C 1997 *The Kondo Problem to Heavy Fermions* (Cambridge: Cambridge University Press)
[9] Sugiyama K, Iga F, Kasaya M, Kasuya T and Date M 1988 *J. Phys. Soc. Japan* **57** 3946–53
[10] Bat'ková M, Bat'ko I, Konovalova E S, Shitsevalova N and Paderno Y 2006 *Physica* B **378** 618–9
[11] Okamura H, Michizawa T, Nanba T, Kimura S I, Iga F and Takabatake T 2005 *J. Phys. Soc. Japan* **74** 1954–7
[12] Ekino T, Umeda H, Iga F, Shimizu N, Takabatake T and Fujii H 1999 *Physica* B **259** 315–6
[13] Iga F, Kasaya M and Kasuya T 1988 *J. Magn. Magn. Mater.* **76–7** 156–8
[14] Iga F, Shimizu N and Takabatake T 1998 *J. Magn. Magn. Mater.* **177–81** 337–8
[15] Schlesinger M E 1998 *J. Phase Equilib. Diffus.* **19** 49–55
[16] Werheit H, Filipov V, Shirai K, Dekura H, Shitsevalova N, Schwarz U and Armbrüster M 2011 *J. Phys.: Condens. Matter* **23** 065403
[17] Blaha P, Schwarz K, Madsen G, Kvasnicka D and Luitz J 2001 *WIEN2k: an Augmented Plane Wave + Local Orbitals Program for Calculating Crystal Properties* (Vienna: Vienna University of Technology Institute of Materials Chemistry)
[18] Tran F and Blaha P 2009 *Phys. Rev. Lett.* **102** 226401
[19] Shoenberg D 1984 *Magnetic Oscillations in Metals* (Cambridge: Cambridge University Press)
[20] Landau L 1957 *Sov. Phys.—JETP* **3** 920–5
[21] Iga F, Suga K, Takeda K, Michimura S, Murakami K, Takabatake T and Kindo K 2010 *J. Phys.: Conf. Ser.* **200** 012064
[22] Weng H, Zhao J, Wang Z, Fang Z and Dai X 2014 *Phys. Rev. Lett.* **112** 016403
[23] Antonov V N, Harmon B N and Yaresko A N 2002 *Phys. Rev.* B **66** 165209
[24] Anderson P W 1992 *Phys. Scr.* T **42** 11–6
[25] Grover T, Trivedi N, Senthil T and Lee P A 2010 *Phys. Rev.* B **81** 245121
[26] Motrunich O I 2006 *Phys. Rev.* B **73** 155115
[27] Katsura H, Nagaosa N and Lee P A 2010 *Phys. Rev. Lett.* **104** 066403
[28] Knolle J and Cooper N R 2017 *Phys. Rev. Lett.* **118** 096604
[29] Chowdhury D, Sodemann I and Senthil T 2017 arXiv:1706.00418
[30] Sodemann I, Chowdhury D and Senthil T 2018 *Phys. Rev.* B **97** 045152
[31] Coleman P, Miranda E and Tsvelik A 1993 *Physica* B **186–8** 362–4
[32] Baskaran G 2015 arXiv:1507.03477
[33] Erten O, Chang P Y, Coleman P and Tsvelik A M 2017 *Phys. Rev. Lett.* **119** 057603
[34] Pixley J, Yu R, Paschen S and Si Q 2015 arXiv:1509.02907
[35] Kagan Y, Kikion K and Prokof'ev N 1992 *Physica* B **182** 201–8
[36] Heinecke M, Winzer K N J K H, Grieb H, Flachbart K and Paderno Y B 1995 *Z. Phys.* B **98** 231–7
[37] Harima H, Yanase A and Kasuya T 1985 *J. Magn. Magn. Mater.* **47–8** 567–9
[38] Okuda N, Suzuki T, Ishii I, Sayaka H, Iga F, Takabatake T, Fujita T, Kadomatsu H and Harima H 2000 *Physica* B **281–2** 756–7
[39] Wolgast S, Eo Y S, Sun K, Kurdak C, Balakirev F F, Jaime M, Kim D J and Fisk Z 2017 *Phys. Rev.* B **95** 245112
[40] Knolle J and Cooper N R 2015 *Phys. Rev. Lett.* **115** 146401
[41] Erten O, Ghaemi P and Coleman P 2016 *Phys. Rev. Lett.* **116** 046403
[42] Xu Y, Cui S, Dong J K, Zhao D, Wu T, Chen X H, Sun K, Yao H and Li S Y 2016 *Phys. Rev. Lett.* **116** 246403
[43] Zhang L, Song X Y and Wang F 2016 *Phys. Rev. Lett.* **116** 046404